ACS Biomaterials SCIENCE & ENGINEERING
Cite This: ACS Biomater. Sci. Eng. XXXX, XXX, XXX−XXX
Article
pubs.acs.org/journal/abseba

Substrate Stiffness, Cell Anisotropy, and Cell−Cell Contact Contribute to Enhanced Structural and Calcium Handling Properties of Human Embryonic Stem Cell-Derived Cardiomyocytes

Marita L. Rodriguez,[†] Kevin M. Beussman,[†] Katherine S. Chun,[†] Melissa S. Walzer,[‡] Xiulan Yang,[‡,§,∥] Charles E. Murry,[‡,§,∥,⊥,#] and Nathan J. Sniadecki*[,†,§,∥,⊥]

[†]Department of Mechanical Engineering, University of Washington, Seattle, Washington 98195, United States
[‡]Department of Pathology, University of Washington, Seattle, Washington 98195, United States
[§]Center for Cardiovascular Biology, University of Washington, Seattle, Washington 98109, United States
[∥]Institute for Stem Cell and Regenerative Medicine, University of Washington, Seattle, Washington 98109, United States
[⊥]Department of Bioengineering, University of Washington, Seattle, Washington 98195, United States
[#]Department of Medicine/Cardiology, University of Washington, Seattle, Washington 98195, United States

Supporting Information

ABSTRACT: Human pluripotent stem cell-derived cardiomyocytes (hPSC-CMs) can be utilized to understand the mechanisms underlying the development and progression of heart disease, as well as to develop better interventions and treatments for this disease. However, these cells are structurally and functionally immature, which undermines some of their adequacy in modeling adult heart tissue. Previous studies with immature cardiomyocytes have shown that altering substrate stiffness, cell anisotropy, and/or cell−cell contact can enhance the contractile and structural maturation of hPSC-CMs. In this study, the structural and calcium handling properties of human embryonic stem cell-derived cardiomyocytes (hESC-CMs) were enhanced by exposure to a downselected combination of these three maturation stimuli. First, hESC-CMs were seeded onto substrates composed of two commercial formulations of polydimethylsiloxane (PDMS), Sylgard 184 and Sylgard 527, whose stiffness ranged from 5 kPa to 101 kPa. Upon analyzing the morphological and calcium transient properties of these cells, it was concluded that a 21 kPa substrate yielded cells with the highest degree of maturation. Next, these PDMS substrates were microcontact-printed with laminin to force the cultured cells into rod-shaped geometries using line patterns that were 12, 18, or 24 μm in width. We found that cells on the 18 and 24 μm pattern widths had structural and functional properties that were superior to those on the 12 μm pattern. The hESC-CMs were then seeded onto these line-stamped surfaces at a density of 500 000 cells per 25-mm-diameter substrate, to enable the formation of cell−cell contacts at their distal ends. We discovered that this combination of culture conditions resulted in cells that were more structurally and functionally mature than those that were only exposed to one or two stimuli. Our results suggest that downselecting a combination of mechanobiological stimuli could prove to be an effective means of maturing hPSC-CMs in vitro.

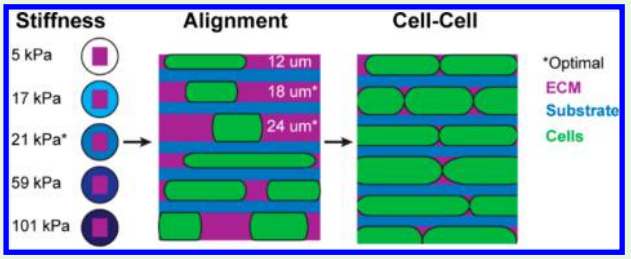

KEYWORDS: *Stiffness, anisotropy, cell−cell contact, maturation, human embryonic stem cell-derived cardiomyocytes (hESC-CMs)*

1. INTRODUCTION

Human pluripotent stem cell-derived cardiomyocytes can be used as replacements for diseased or dead tissue in the heart, to assess pharmacological treatments for heart disease, and to model different developmental and pathological states of the heart.[1] However, to serve these roles effectively, hPSC-CMs should mimic the developmental state of the cells that they are meant to model or replace. Unfortunately, hPSC-CMs have distinctly immature electrophysiological, structural, and mechanical properties that undermine their use in these studies.[2] To effectively utilize the potential that hPSC-CMs can offer, they must first be matured to a more adultlike cell state prior to experimentation.[3]

Previous studies with immature cardiomyocytes have shown enhanced maturation using several different methods. Prolonged cell culture is one of the most common techniques, which involves allowing the cells to grow in culture for an extended period of time.[4−8] Alternatively, cell biophysical pathways can be activated via cues such as cell anisotropy,[9−17] cell−cell contact,[18,19] substrate stiffness,[20−27] applied mechan-

Special Issue: Biomaterials for Mechanobiology

Received: October 12, 2018
Accepted: February 6, 2019
Published: February 6, 2019

DOI: 10.1021/acsbiomaterials.8b01256
ACS Biomater. Sci. Eng. XXXX, XXX, XXX−XXX

ical strain,[28−39] or electrical pacing.[40−44] Pharmacological and viral biochemical agents have also been found to enhance the maturation of immature cardiomyocytes.[45−53] While many of these developmental cues have been investigated, it would be beneficial to clarify the impact of these individual stimuli, or combinations of these stimuli, on hPSC-CM structure and function.

Advanced custom culture environments have been used to study the effect of simultaneously applying two or more stimuli to the hPSC-CM culture environment.[54−57] These studies have discovered that a combination of pro-maturation stimuli, e.g., anisotropy and stiffness, can have compounding effects on cardiomyocyte maturation. Based on these results, we hypothesized that a downselected combination of these techniques could be used to quickly advance hPSC-CM maturation to a more adultlike phenotype. To examine this hypothesis, we assessed the functional and structural enhancement of hESC-CMs under combinations of three mechanobiological stimuli: substrate stiffness, cell anisotropy, and cell−cell contact.

2. MATERIALS AND METHODS

2.1. Cell Culture. Undifferentiated GCaMP3-expressing RUES2 hESCs[58] were cultured with mouse embryonic fibroblast conditioned media supplemented with basic fibroblast growth factor (R&D Systems). Cardiac differentiation of the cells was based on a previously published directed differentiation protocol[59] (Figure 1).

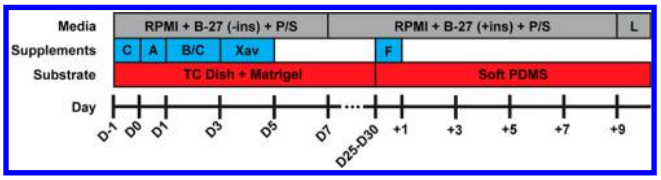

Figure 1. Cell culture protocol. Time course of media, supplements, and culture substrates used for these experiments. [Legend: ins, insulin; P/S, penicillin/streptomysin; L, live cell-imaging media; C, CHIR 99021; A, Activin A; B, BMP 4; Xav, Xav 939; and F, fetal bovine serum.]

Briefly, after plating in a monolayer, the cultures were switched to RPMI media (Gibco) supplemented with B-27 minus insulin (Gibco), activin A (R&D Systems), and Matrigel (Corning Life Science). This was followed by subsequent feedings supplemented with BMP4 (R&D Systems) and CHIR 99021 (Cayman Chemical), followed by Xav 939 (Tocris Bioscience). After 20 days of directed differentiation, cells were treated with a "pro-survival cocktail" containing:[60] Matrigel supplemented with 100 mM benzyloxycarbonyl-Val-Ala-Asp(O-methyl)-fluoromethyl ketone (Calbiochem), 50 nM Bcl-XL BH4 (Calbiochem), 200 nM cyclosporine A (Wako Pure Chemicals), 100 ng/mL IGF-1 (Peprotech), and 50 mM pinacidil (Sigma−Aldrich); and were then cryopreserved.[61] Dissociated cells were seeded at a density of ∼250 000 cells per 25-mm-diameter substrate (500 000 cells for experiments on cell−cell contact) in RPMI medium supplemented with 10% fetal bovine serum (Life Technologies). The following day, the culture media was removed and replaced with serum-free RPMI, which was exchanged every other day.

2.2. Preparation of Soft Silicone Substrates. PDMS substrates were created with stiffnesses that span the physiological range from normal to pathophysiological for cardiac tissue[20−22,62] (see Figure 2A). These substrates were made by combining Sylgard 184 (prepared at a 10:1 ratio) and Sylgard 527 (Dow Corning) (prepared at a 1:1 ratio) to yield PDMS mixtures of 0%, 5%, 10%, 15%, and 20% Sylgard 184 by weight.[63] Following mixing and degassing, the PDMS mixtures were poured onto round No. 1 glass coverslips (VWR) that

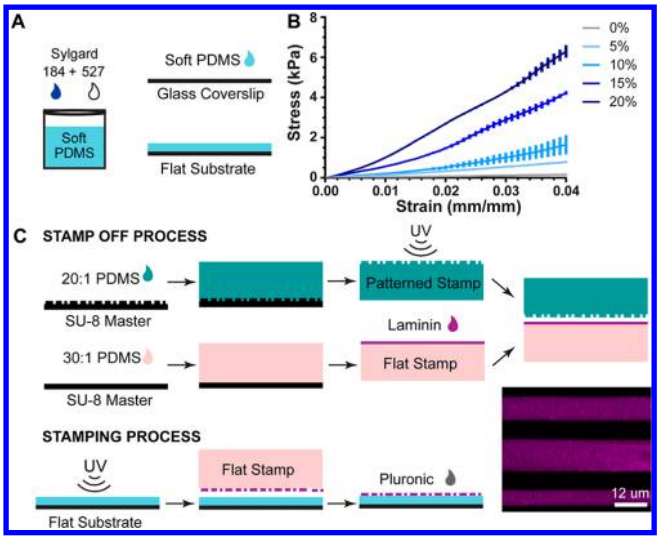

Figure 2. Fabrication and characterization of soft PDMS substrates. (A) Soft PDMS substrates of different stiffnesses were made by coating mixtures of Sylgard 184 and Sylgard 527 onto glass coverslips. (B) Stress−strain curves for cylindrical samples of soft PDMS were obtained from compression tests and were used to determine the Young's modulus for each sample mixture by calculating the slope of the stress−strain curve in the linear portion of each data set. (C) To produce soft PDMS substrates with patterned lines of laminin, a mixture of 20:1 Sylgard 184 was cured on a SU-8 silicon wafer that contained a negative copy of the desired line pattern. This patterned stamp was then used to selectively remove protein that has been absorbed to a 30:1 Sylgard 184 flat stamp. The protein pattern on the flat stamp is transferred to a UV-treated soft PDMS substrate by bringing the two into contact. Once the pattern has been transferred, the remaining surfaces of the substrate are coated with Pluronic to restrict cell attachment to the patterned lines.

were pretreated with oxygen plasma (SPI Supplies). The liquid PDMS was cured in an oven at 65 °C for 20−24 h. Cured substrates were then exposed to UV light (Jelight Company, Inc.) for 7 min to activate their surfaces for protein transfer via microcontact printing.

2.3. Mechanical Characterization of Soft PDMS Substrates. The Young's modulus of each PDMS mixture was experimentally determined by compression tests using an Instron 5585H Universal Testing System (Instron Corp.). Compression samples were cylindrical in shape, being 25 mm in diameter and 15−20 mm in height. During testing, a constant strain of 1 mm/s was applied to all samples and the corresponding stress was evaluated using Bluehill 3 Testing Software (Figure 2B). Young's moduli were then calculated from the linear portion of the stress−strain curves between a strain value of 0 and 0.15 and averaged across three replicate experiments.

2.4. Stamp Fabrication and Stamping Process. For all substrates, 150 μL of 50 μg/mL mouse laminin (Life Technologies) was absorbed onto a flat PDMS stamp for 1 h. For unpatterned surfaces, this stamp was then placed in direct contact with a UV-treated soft PDMS substrate. Surfaces with line patterns of laminin were created using a stamp-off technique[64] (Figure 2C). LayoutEditor software (layouteditor.com) was used to design a stamp containing lines 12, 18, and 24 μm wide. To prevent cells from bridging across these patterns, the gap between adjacent lines was designed to be 20 μm. SU-8 (MicroChem) versions of these patterned stamps were fabricated via photolithography processes, as previously described.[65] The resulting SU-8 master was used to make identical negative copies of the line pattern by preparing Sylgard 184 PDMS (Dow Corning) in a 20:1 (base-to-curing agent) ratio, degassing this mixture, pouring it over the master, and curing the PDMS in a 110 °C oven for 10 min. Flat stamps were made in a similar manner by casting a 30:1 PDMS mixture on a clean, pattern-free silicon wafer. The resulting flat PDMS was then cut into 1 cm × 1 cm square stamps, which were then coated

DOI: 10.1021/acsbiomaterials.8b01256
ACS Biomater. Sci. Eng. XXXX, XXX, XXX−XXX

with a layer of laminin (50 μg/mL). Protein regions were then selectively removed from the flat stamp by bringing the UV-activated patterned stamp into contact with its protein-absorbed surface. This flat stamp was then brought into contact with the UV-activated substrate, leaving behind the laminin line pattern.

2.5. Immunofluorescence Imaging. Following live experiments, the cells were fixed to their underlying substrate and stained to assess their morphological and structural state. Cells were fixed in a solution of 4% paraformaldehyde (EMD Chemicals) in phosphate-buffered saline (PBS). Prior to staining, the cells were permeabilized by immersing the substrates in 0.5% Triton X-100 surfactant (EMD Chemicals) for 10 min. Cell nuclei were stained with Hoechst 33342 (Life Technologies), while sarcomeric α-actinin was tagged with monoclonal mouse anti-α-actinin (Sigma–Aldrich) and stained with goat antimouse AlexaFluor 488 (Life Technologies). In addition, patterned regions of laminin on top of the soft PDMS were treated with rabbit antilaminin (Sigma–Aldrich) and stained with a goat antirabbit AlexaFluor 647 (Life Technologies).

2.6. Calcium Imaging. For live calcium transient imaging, cell media was replaced with Krebs-Henseleit buffer equilibrated at 95% O_2 and 5% CO_2 a week following cell seeding. Calcium transients in beating GCaMP3 hESC-CMs were recorded using a Hamamatsu ORCA-Flash2.8 Scientific CMOS camera fitted on a Nikon Eclipse Ti upright microscope. All videos were taken at 40× magnification, using a water immersion objective. In addition, a live cell chamber was used to maintain the cells at 37 °C throughout the imaging process.

2.7. Structural Analysis. Differences in cellular spread area, aspect ratio, multinucleation percentage, nuclear volume, sarcomere length, and Z-band width were assessed using ImageJ for all fixed and stained cells (Figure 3A). These properties were assessed on a per-cell basis for both individual hESC-CMs and those grown in cell–cell contact. For cell–cell contact studies, cellular interaction was confirmed by the presence of myofibrils which continued from one cell to another. To calculate average sarcomere lengths, the Plot Profile function was used to determine the average sarcomere length across at least five parallel Z-bands, at three different locations throughout the cell. These values were then averaged together to yield the average sarcomere length for each cell. For Z-band width measurements, we used the Fast Filter, Despeckle, Remove Outliers, and Binary functions to define the borders of individual Z-bands. Groups of at least five parallel Z-bands at three different locations throughout the cell were analyzed using the Analyze Particles function to find the major axis of each Z-band. These values were then summed together to determine the average Z-band width value for each cell.

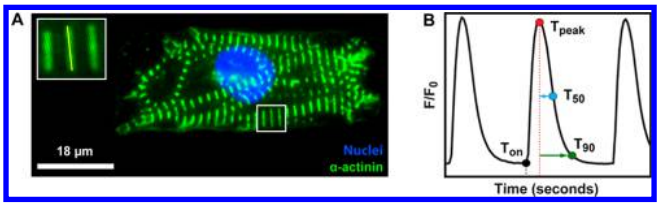

Figure 3. Analysis methods. (A) Example immunofluorescent image of hESC-CM on a 20 kPa soft PDMS substrate (inset shows a high-magnification view of cell sarcomeres, where the length of the yellow line indicates a single measurement of Z-band width). (B) Representative calcium trace, where the times at which the signal initiates (T_{on}, black), reaches its peak value (T_{peak}, red), decays to 50% of the peak value (T_{50}, blue), and decays to 90% of the peak value (T_{90}, green) are indicated. The rate of calcium release (R_{peak}) is the slope of the graph between time points T_{on} and T_{peak}, the rate of 50% calcium reuptake is the slope between T_{peak} and T_{50}, and the rate of 90% calcium reuptake is the slope between T_{peak} and T_{90}.

2.8. Calcium Transient Analysis. All calcium transients were analyzed on a per-cell basis, using a custom-written MATLAB code. For cell–cell contact studies, cellular interaction was confirmed by calcium transient synchrony. For each cell, the video frame with the maximum average pixel intensity was identified and used to obtain the cell boundary with thresholding and edge detection techniques. The calcium signal intensity was then assessed by averaging the pixel intensity within the defined cell boundary for each frame of the video. The background signal intensity was determined by measuring the fluorescent signal in an area far from the cell. The peak intensity (F) and baseline intensity (F_0) were then normalized by subtracting this background signal, and the normalized intensity ratio was determined using the following equation:

$$\frac{F}{F_0} = \frac{F_{max} - F_{background}}{F_{baseline} - F_{background}} \quad (1)$$

To determine differences in calcium transient properties between cell groups, the normalized baseline intensity (F_0), normalized maximal intensity (F), normalized intensity ratio (F/F_0), time to peak intensity (T_{peak}), time to 50% calcium reuptake (T_{50}), time to 90% calcium reuptake (T_{90}), and the rates of calcium release (R_{peak}), 50% reuptake (R_{50}), and 90% reuptake (R_{90}) were analyzed (Figure 3B), where

$$R_{peak} = \frac{F/F_0}{T_{peak} - T_{on}} \quad (2)$$

$$R_{50} = \frac{0.5F/F_0}{T_{50} - T_{peak}} \quad (3)$$

$$R_{90} = \frac{0.9F/F_0}{T_{90} - T_{peak}} \quad (4)$$

2.9. Statistical Analysis. Because of the nonparametric nature of the data resulting from these studies, statistical differences in the tested datasets were assessed using a Kruskal–Wallis ANOVA on Ranks. Statistical differences between conditions were performed using Dunn's post hoc test with a correction for multiple comparisons. Because of the binary nature of the multinucleation data, standard error could not be computed and multiple treatments were compared with Fisher's test. These data are depicted graphically as scatter plots containing experimental averages. Statistical significance was assessed at $p < 0.05$ and is denoted in the figures presented in this work by horizontal lines, where a single asterisk (*) denotes $p < 0.05$, two asterisks (**) denote $p < 0.01$, three asterisks (***) denote $p < 0.005$, and four asterisks (****) denote $p < 0.001$. Box and whisker plots contain 5%–95% of the analyzed data, with the outliers shown as black dots. The cross symbol (+) indicates the mean of the data.

3. RESULTS

3.1. Stiffness. The stress and strain data obtained from compression testing was used to determine the compressive moduli of the soft silicone samples made by mixing Sylgard 184 and Sylgard 527. Young's moduli were then calculated from the linear portion of the stress–strain curves and averaged across three replicate experiments. The resulting moduli were calculated to be 4.5 ± 0.8, 16.6 ± 2.7, 21.0 ± 1.8, 58.8 ± 2.2, and 101.3 ± 9.9 kPa, for 0%, 5%, 10%, 15%, and 20% Sylgard 184 mixtures, respectively.

Upon analyzing fixed and stained images of unpatterned hESC-CMs on soft PDMS substrates of different stiffnesses (Figure 4), it was observed that cell area, multinucleation, and the nuclear volume fraction all showed significant trends based on substrate stiffnesses. Specifically, cell area was highest on the 21 kPa substrate and decreased with increasing or decreasing stiffness. This same substrate stiffness was also found to have the highest degree of cell binucleation, as well as the lowest nuclei-to-cellular volume ratio. However, substrate stiffness did not have a significant effect on cell aspect ratio, Z-band width, or sarcomere length.

DOI: 10.1021/acsbiomaterials.8b01256
ACS Biomater. Sci. Eng. XXXX, XXX, XXX–XXX

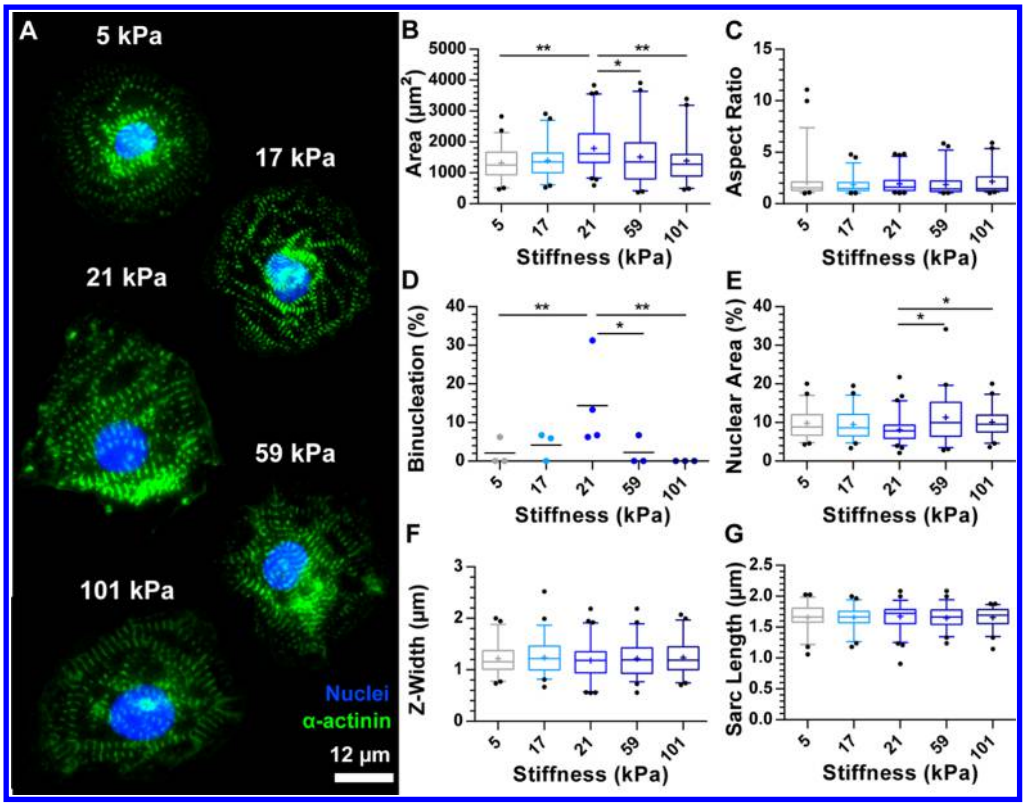

Figure 4. Effect of substrate stiffness on the structural state of hESC-CMs. (A) Representative immunofluorescent images of hESC-CMs on unpatterned soft PDMS substrates of different stiffnesses. These images were analyzed to quantify (B) cell spread area, (C) cell aspect ratio, (D) percentage of binucleated cells, (E) percent of total cell area occupied by the nucleus, (F) Z-band width, and (G) sarcomere length. Lines on graphs indicate significance at $p < 0.05$ ((*) $p < 0.05$, (**) $p < 0.01$, (***) $p < 0.005$, and (****) $p < 0.001$). Data compiled from $N = 3$ experiments and at least $n = 45$ cells per condition.

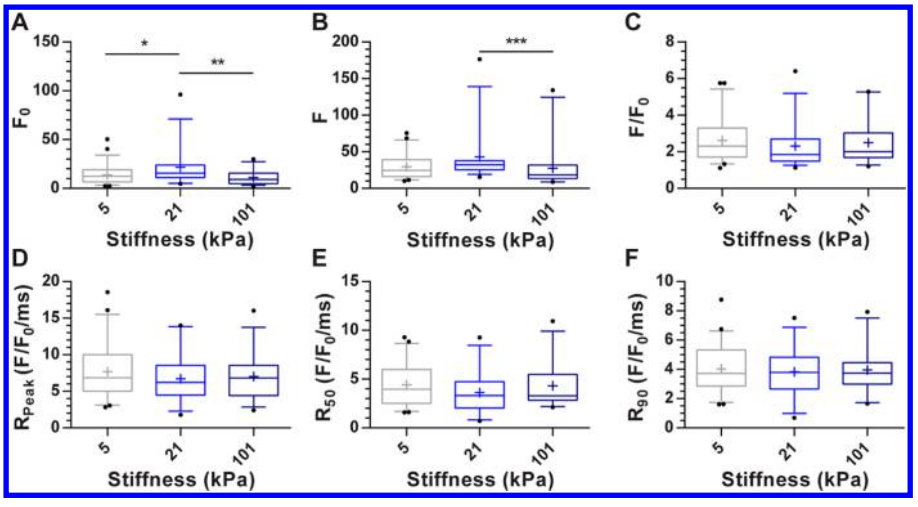

Figure 5. Effect of substrate stiffness on hESC-CM calcium transients. Shown here are the analyzed parameters of (A) normalized baseline calcium signal, (B) normalized maximum calcium intensity signal, (C) normalized intensity ratio, and the rates of (D) calcium release, (E) 50% calcium reuptake, and (F) 90% calcium reuptake. Lines on graphs indicate significance at $p < 0.05$ ((*) $p < 0.05$, (**) $p < 0.01$, (***) $p < 0.005$, and (****) $p < 0.001$). Data compiled from $N = 3$ experiments and at least $n = 30$ cells per condition.

Calcium transient analysis for cells on the 5, 21, and 101 kPa substrates revealed that basal and maximal values of calcium were significantly higher on the 21 kPa substrate (Figures 5A and 5B), but no significant difference in the ratio of these values was found (Figure 5C). The rates of calcium release, 50% reuptake, and 90% reuptake were not different for cells seeded on substrates of different stiffnesses (Figures 5D–F). In addition, there was no significant difference in the timing of calcium transients (T_{peak}, T_{50}, T_{90}) for these cells (Table 1), indicating little or no dependence of these properties on substrate stiffness. Together, the results from our morphological and calcium analyses indicate that the 21 kPa substrate served as the best culture substrate for promoting the structural enhancement of hESC-CMs. As such, this substrate stiffness was used for all the following experiments.

DOI: 10.1021/acsbiomaterials.8b01256
ACS Biomater. Sci. Eng. XXXX, XXX, XXX–XXX

Table 1. Time Course of Calcium Transients for hESC-CMs on Substrates of Varying Stiffness[a]

	5 kPa	21 kPa	101 kPa
T_{peak} (ms)	414.02 ± 39.95	389.21 ± 35.71	391.83 ± 36.83
T_{50} (ms)	351.08 ± 30.70	413.99 ± 56.89	314.47 ± 20.66
T_{90} (ms)	675.1 ± 58.13	652.59 ± 82.42	603.65 ± 42.87

[a] T_{peak} is the time to peak signal intensity, T_{50} is the time from peak signal intensity to 50% signal decay, and T_{90} is the time to 90% signal decay. Transient times are given as mean time ± standard error. No significant differences were found between the three tested stiffness conditions for $p < 0.05$. Data compiled from $N = 3$ experiments and at least $n = 30$ cells per condition.

3.2. Anisotropy. The effect of cell anisotropy on the structural and functional enhancement of individual RUES2 hESC-CMs was assessed by using a stamp-off technique to pattern lines of laminin onto 21 kPa soft PDMS surfaces. Three different pattern widths of 12, 18, and 24 μm were chosen in accordance with previous studies on cell anisotropy.[9,66−69] Following a week of culture on these substrates, aligned and nonaligned cells on the same substrate were analyzed and compared to determine the effects of forced anisotropy on the structural and calcium handling properties of these cells.

The capability of the stamp-off and microcontact printing techniques to transfer lines of 12, 18, and 24 μm wide lines of laminin onto soft PDMS surfaces was assessed by immunofluorescent staining. The impact of substrate stiffness on deposited laminin concentration was measured by quantitatively assessing the intensity of immunofluorescence antibody staining (Figure S1 in the Supporting Information) but no distinguishable trend was found. In addition, there was no significant difference in laminin concentration for different pattern widths (Figure S2 in the Supporting Information).

Several significant changes in cell organization and morphology were found upon forcing hESC-CMs to adopt an elongated cell morphology via microcontact printing (see Figure 6). Cell area significantly decreased with decreasing pattern width (Figure 6B), while the opposite relationship held for cell aspect ratio (Figure 6C). Upon quantifying the number of nuclei within patterned cells, we found that binucleation was not significantly different among cells on different pattern widths (Figure 6D), but the percentage of the cell volume occupied by these nuclei significantly increased with decreasing pattern width (Figure 6E). Lastly, Z-band widths were highest on the 18 and 24 μm width patterns (Figure 6F), and sarcomere length and alignment were both found to increase as the pattern width decreased (see Figure 6G, as well as Figure S3 in the Supporting Information).

Recent studies have found that, on moderately stiff culture substrates (10−35 kPa), force generation is maximal in myocytes that have an aspect ratio of ∼7:1, and as substrate stiffness increases, this optimal aspect ratio decreases.[10] Since cells on the 12 μm pattern width had average aspect ratios ranging from 8 to 10 and often had nuclei that spanned the entire cell width (which is not ideal for calcium imaging), calcium transients were only examined for unpatterned cells and cells on the 18 and 24 μm wide patterns (see Figure 7).

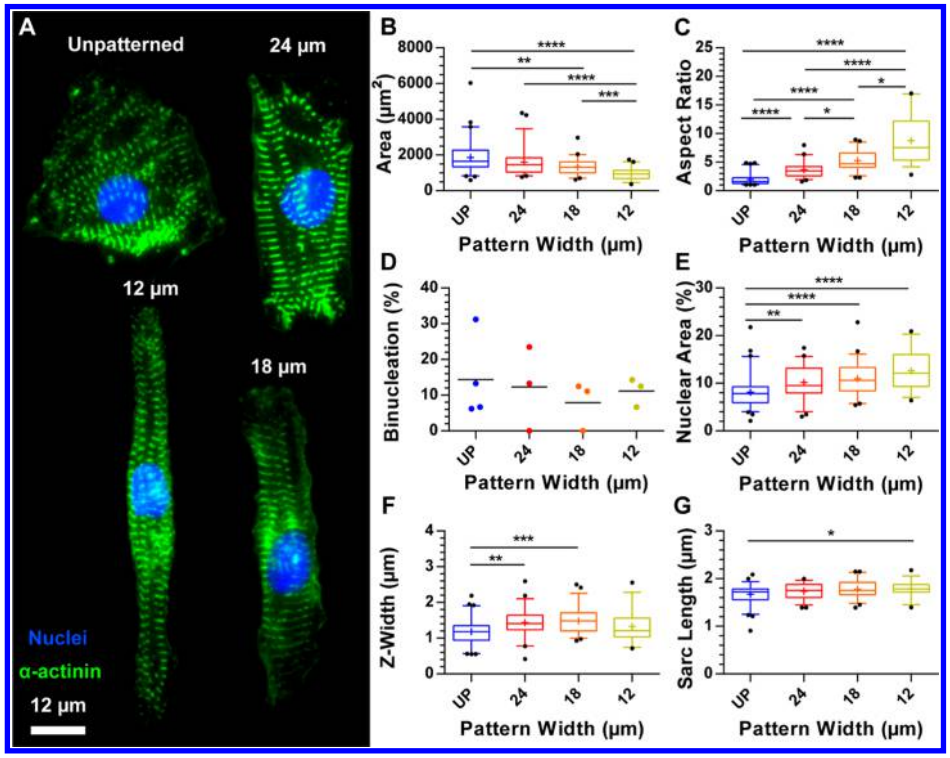

Figure 6. Effect of alignment on the structural maturation of hESC-CMs. (A) Representative immunofluorescent images of hESC-CMs on 21 kPa soft PDMS substrates patterned with 12, 18, and 24 μm wide lines of laminin. An unpatterned cell from a substrate of the same stiffness is shown for reference. These images were analyzed to assess differences in (B) cell spread area, (C) cell aspect ratio, (D) percentage of binucleated cells, (E) percent of total cell area occupied by the nucleus, (F) Z-band width, and (G) sarcomere length. Lines on graphs indicate significance at $p < 0.05$ ((*) $p < 0.05$, (**) $p < 0.01$, (***) $p < 0.005$, and (****) $p < 0.001$). Data compiled from $N = 3$ experiments and at least $n = 35$ cells per condition.

DOI: 10.1021/acsbiomaterials.8b01256
ACS Biomater. Sci. Eng. XXXX, XXX, XXX−XXX

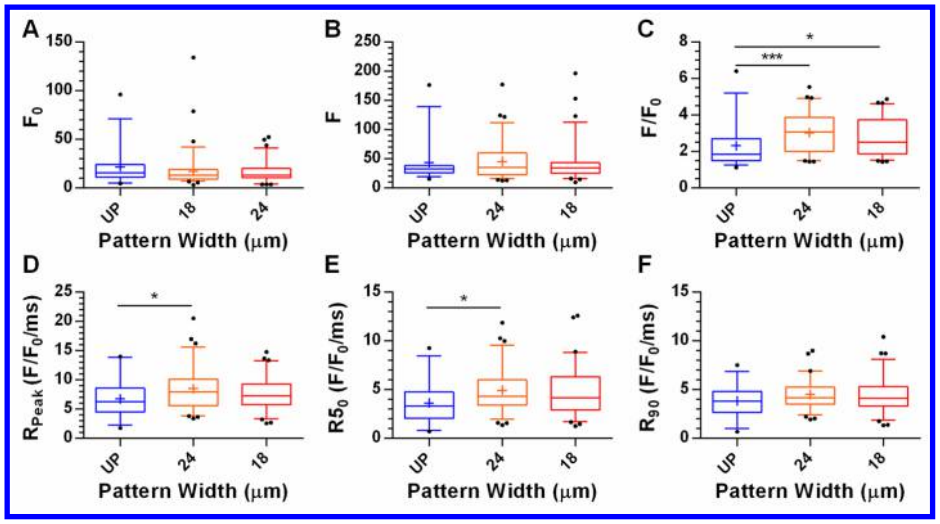

Figure 7. Effect of cell anisotropy on hESC-CM calcium transients. Shown here are the analyzed parameters of (A) normalized baseline calcium signal, (B) normalized maximum calcium intensity signal, (C) normalized intensity ratio, and the rates of (D) calcium release, (E) 50% calcium reuptake, and (F) 90% calcium reuptake. Lines on graphs indicate significance at $p < 0.05$ ((*) $p < 0.05$, (**) $p < 0.01$, (***) $p < 0.005$, and (****) $p < 0.001$). Data compiled from $N = 3$ experiments and at least $n = 30$ cells per condition.

Analysis of these transients revealed that, although there was no significant difference in basal intensity (Figure 7A) or maximal intensity (Figure 7B), hESC-CMs aligned on either 18 or 24 μm patterns had significantly higher maximum-to-basal calcium intensity ratios, when compared to unpatterned hESC-CMs (Figure 7C). Anisotropy also led to increases in the rates of calcium release (Figure 7D), 50% signal decay (Figure 7E), and 90% signal decay (Figure 7F). Lastly, there were no significant differences in the timing of calcium transients (Table 2). Together, these results indicate that

Table 2. Time Course of Calcium Transients for Unpatterned and Patterned hESC-CMs[a]

	unpatterned	24 μm	18 μm
T_{peak} (ms)	389.21 ± 35.71	403.15 ± 22.62	405.36 ± 22.89
T_{50} (ms)	413.99 ± 56.89	346.45 ± 18.89	351.67 ± 22.48
T_{90} (ms)	652.59 ± 82.42	646.22 ± 29.96	642.72 ± 35.81

[a] T_{peak} is the time to peak signal intensity, T_{50} is the time from peak signal intensity to 50% signal decay, and T_{90} is the time to 90% signal decay. Transient times are given as mean time ± standard error. No significant differences were found between the three tested conditions $p < 0.5$. Data compiled from $N = 3$ experiments and at least $n = 30$ cells per condition.

pattern widths of less than 18 μm patterns result in cells with higher than optimal aspect ratios, and those patterns larger than 24 μm result in cells with poor sarcomeric structure, suggesting that intermediate pattern widths are better suited for growing and maturing hPSC-CMs. In addition, cell anisotropy appears to have a positive effect on the calcium transient properties of these cells.

3.3. Cell–Cell Contact. To determine the effect of cell–cell contact on hESC-CMs, RUES2 hESC-CMs were seeded at a high density onto 18 and 24 μm patterned lines of laminin and allowed to form one-dimensional strips of cardiomyocytes. Following a week of culture on these substrates, the same properties described in our stiffness and cell anisotropy studies were assessed, on a single-cell basis, to determine the effect of cell–cell contact on the structural and functional state of these cells (see Figure 8).

We found that cell–cell contact within 24-μm width patterns led to significant increases in cell spread area, when compared to single cells or lines of cells on the 18-μm pattern width (Figure 8B). Although aspect ratios were still low on average, cell–cell contact was able to produce increases in these values (Figure 8C). The strongest effect of cell–cell contact was a significant increase in the percentage of binucleated cells on the 24-μm width pattern, compared to all other conditions (Figure 8D). In addition, the nuclear area percentage decreased with cell–cell contact (Figure 8E). Upon investigating the cytoskeletal structure of these cells, Z-band width was found to significantly decrease with cell–cell contact on both pattern widths (Figure 8F), and sarcomere length significantly increased on the 18-μm pattern width under cell–cell contact, when compared to single cells on the 24-μm pattern width (Figure 8G).

Calcium transient analysis of single isolated cells and cells in contact with neighboring cardiomyocytes (Figure 9) revealed that cell–cell contact resulted in slight increases to the normalized basal (Figure 9A) and maximal (Figure 9B) calcium intensity, and significant decreases in the maximal to basal intensity ratio (Figure 9C). For the most part, the rates of calcium release and uptake increased, but these changes were not found to be significant (Figures 9E–G). However, cell–cell contact did result in significantly faster calcium transient kinetics (see Table 3). Akin to the single-cell anisotropy study, cell–cell groups on the 24-μm width pattern had shorter transient times than on the 18-μm width. Taken together, these results suggest that cell–cell contact plays a role in both the structural and functional enhancement of hPSC-CMs, and advocates for growing these cells as such.

4. DISCUSSION

In this work, a downselected combination of substrate stiffness, laminin pattern width, and cell–cell contact was employed to enhance the structural and functional properties of hESC-CMs. The order in which these stimuli were assessed was chosen based upon simplicity and optimization of the culture environment. One of the most basic necessities of adherent cell culture is the establishment of a culture surface, which

DOI: 10.1021/acsbiomaterials.8b01256
ACS Biomater. Sci. Eng. XXXX, XXX, XXX–XXX

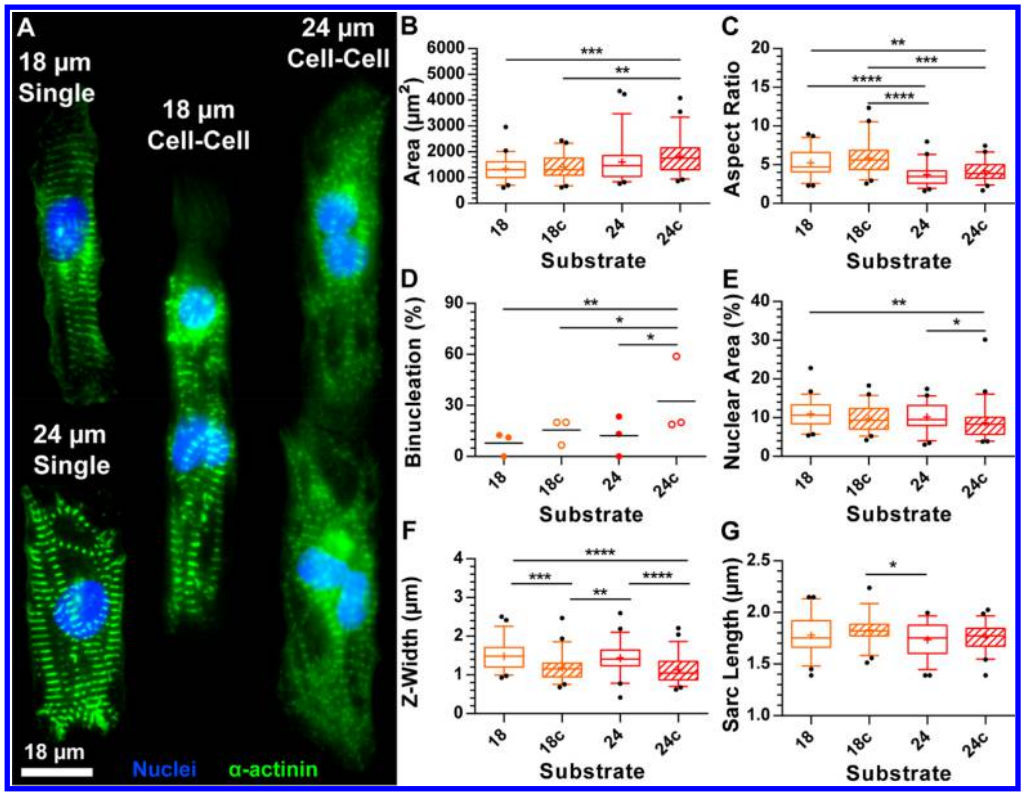

Figure 8. Effect of cell−cell contact on the structural state of hESC-CMs. (A) Representative immunofluorescent images of single hESC-CMs and hESC-CMs belonging to a cell-pair on 21 kPa soft PDMS substrates, line-stamped with 12 and 18 μm wide bands of laminin. Quantification of these images was used to assess for differences in (B) cell spread area, (C) cell aspect ratio, (D) percentage of binucleated cells, (E) percent of total cell area occupied by the nucleus, (F) Z-band width, and (G) sarcomere length. A lowercase c indicates cells from cell-pairs. Lines on graphs indicate significance at $p < 0.05$ ((*) $p < 0.05$, (**) $p < 0.01$, (***) $p < 0.005$, and (****) $p < 0.001$). Data compiled from $N = 3$ experiments and at least $n = 35$ cells per condition.

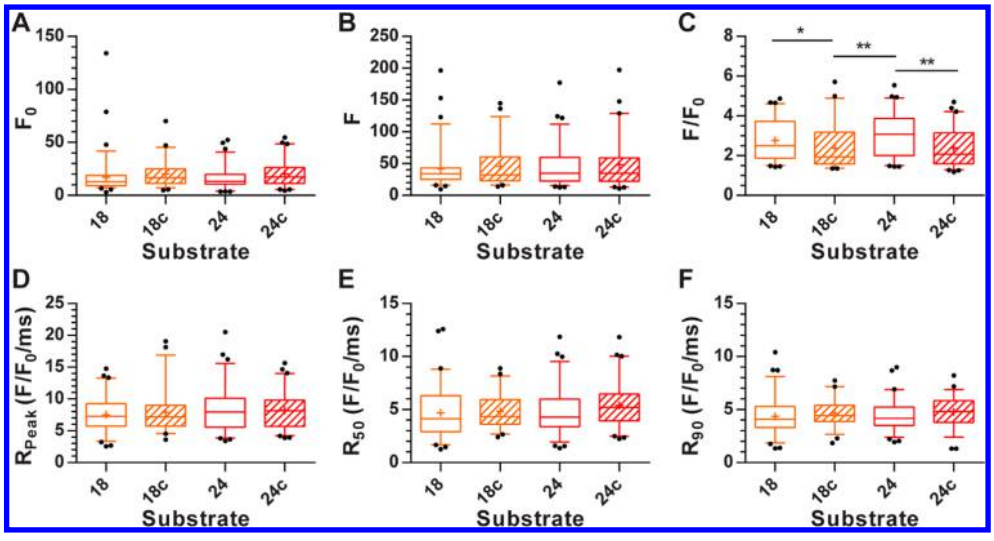

Figure 9. Effect of cell−cell contact on hESC-CM calcium transients. Shown here are the analyzed parameters of (A) normalized baseline calcium signal, (B) normalized maximum calcium intensity signal, and (C) normalized intensity ratio, and the rates of (D) calcium release, (E) 50% calcium reuptake, and (F) 90% calcium reuptake. Lines on graphs indicate significance at $p < 0.05$ ((*) $p < 0.05$, (**) $p < 0.01$, (***) $p < 0.005$, and (****) $p < 0.001$). Data compiled from $N = 3$ experiments, and at least $n = 58$ cells per condition.

subsequently dictates the environmental stiffness. As such, this was the first variable that we assessed. Once we had established the optimal substrate stiffness, cellular anisotropy was controlled by restricting cell adhesion to micropatterned lines of laminin. Multicellular strands of hESC-CMs were then produced by culturing cells at a high density on these cell-adhesive patterned lines. The choice to culture these cells in lines rather than monolayers was primarily motivated by the desire to create a well-controlled setting in which to study the effects of cell−cell contact on the structural and functional properties of these cells. Patterning the hESC-CMs into lines enabled us to restrict the length of the cell−cell contact area

DOI: 10.1021/acsbiomaterials.8b01256
ACS Biomater. Sci. Eng. XXXX, XXX, XXX−XXX

Table 3. Time Course of Calcium Transients for hESC-CMs in Cell−Cell Contact[a]

	18 μm	18 μm C	24 μm	24 μm C
T_{peak} (ms)	405.36 ± 22.86	325.80[c] ± 20.37	403.15 ± 22.62	295.04[c] ± 10.74
T_{50} (ms)	351.67 ± 22.48	258.36[b,c] ± 13.74	346.45 ± 18.89	229.85[b,c] ± 8.88
T_{90} (ms)	642.72 ± 35.81	498.86[b,c] ± 36.74	646.22 ± 29.96	469.23[b,c] ± 25.13

[a] T_{peak} is the time to peak signal intensity, T_{50} is the time from peak signal intensity to 50% signal decay, and T_{90} is the time to 90% signal decay. Here, the letter C indicates hPSC-CMs in cell−cell contact. Transient times are given as mean time ± standard error. Significant decreases were found between individual aligned cells and those in cell−cell contact for both patterned widths. Data compiled from N = 3 experiments, and at least n = 58 cells per condition. [b]A significant difference from the 18-μm substrate was observed. [c]A significant difference from the 24-μm substrate was observed.

and narrow the directionality of the calcium propagation signal to nearly one-dimensional. Furthermore, work by Feinberg et al. has demonstrated that patterned lines of NRVMs have improved structural and functional maturation, when compared to anisotropically patterned monolayers of cells.[9]

4.1. Stiffness. Depending on the selected cell line, previous studies have found that hPSC-CMs perform best when cultured on substrates with rigidities somewhere in the range of 10−50 kPa,[57,70,71] which coincides with physiological values of myocardial stiffness. To determine the optimal substrate stiffness for our cell line and chosen substrate material (soft PDMS-coated glass coverslips), we chose to study an even wider range of stiffnesses, from 5 kPa to 101 kPa. Upon analyzing the structure of RUES2 hESC-CMs cultured on these substrates, we found that the cell aspect ratio, Z-band width, and sarcomere length were not affected by substrate stiffness (see Figure 4). However, cell spread area and binucleation were significantly higher on the 21 kPa substrate. These results agree with studies examining the effect of substrate stiffness on the structural enhancement of other immature cardiomyocyte lines.

In the mature adult heart, ∼74% of cardiomyocytes have a single nucleus, which occupies ∼5% of the cellular volume.[72,73] The remaining 26% of the adult cardiomyocytes are binucleated, which is significantly higher than the 4.2% that was previously found for human-stem cell-derived cardiomyocytes.[73] The effect of substrate stiffness on hPSC-CM binucleation is not an extensively studied topic; however, in a recent study, increased numbers of binucleated cells and larger spread areas were found in cultures of hPSC-CMs grown on Matrigel-coated PDMS substrates, when compared to those on Matrigel-coated glass.[25] We also discovered that cell binucleation and spread area were most prevalent in cardiomyocytes grown on substrates with physiological values of stiffness. These results suggest that binucleation is affected by substrate stiffness and may be linked to cell hypertrophy.

It has previously been observed that culture substrates that are too stiff or too soft can result in cardiomyocytes with poor sarcomeric organization[21,74−76] and cell spreading,[57,77,78] because of a discrepancy between external and internal forces. If myosin formation is inhibited via the rigidity of the culture surface and a cell is not able to contract, sarcomeres appear scattered, punctate, and misaligned, and the cell is unable to spread.[79] Similarly, if cardiomyocytes are grown on surfaces with a stiffness of less than ∼1 kPa, cell contractile forces are low, resulting in underdeveloped sarcomeres and low cell spreading.[21,74] We found that sarcomere length and Z-band width were not significantly different in cardiomyocytes grown on substrates with stiffnesses between 5 kPa and 101 kPa, implying that our range of stiffness did not impede nor augment sarcomere registry. These results have also been observed in neonatal rat ventricular myocytes (NRVMs)[80] and adult cardiomyocytes.[23] However, we did observe an effect of substrate stiffness on cell spreading. We found that cells seeded on the 21 kPa substrates spread the furthest, and that increasing or decreasing the stiffness of the substrate from this value resulted in cells with smaller spread areas. These results suggest that the external force supplied by the 21 kPa soft PDMS-coated glass is balanced by the internal force-producing capability of the cells employed in these studies. This value is slightly higher than the 5−15 kPa surfaces commonly found to elicit hPSC-CMs[71] and NRVMs[21,81−83] with improved structure, but it is in the range of adult murine heart stiffness.[82]

Previous studies with NRVMs have found that basal calcium, maximal calcium, and the calcium intensity ratio are highest at a midrange stiffness of 10−15 kPa.[21,83] We found that cells seeded onto substrates with an intermediate stiffness of 21 kPa had the highest normalized baseline and maximal calcium intensities, but that there was no difference in the intensity ratio. This finding suggests that cells on the soft PDMS substrates with intermediate stiffness were able to store more calcium than those on softer or stiffer substrates, but the relative amount of calcium being released was the same. This may also explain why the average calcium reuptake rate for these cells was slower, simply because there was more calcium to reabsorb. We also discovered no effect of substrate stiffness on calcium transient times. One study found that the time from calcium signal onset to 90% signal decay in NRVMs significantly decreased on 15 kPa micropost substrates, when compared to those measured for cells on 3 kPa microposts.[83] However, since this measurement was done on a lower range of stiffnesses, it is unclear whether these results disagree with our own. Another study on adult rat cardiomyocytes found that, in the range of 8 kPa to >100 kPa, there was no effect of substrate stiffness on the time to peak calcium signal.[23] These results are in agreement with our findings.

4.2. Anisotropy. In the adult heart, cardiomyocytes are elongated and oriented in parallel with each other. In addition, the ECM environment within the heart is composed of layers of well-organized and aligned protein fibers, which may help to guide myocardial alignment during development and tissue remodeling via nanoscale topographical cues. This organization facilitates both force production, through the orientation of its contractile proteins, as well as electrical signal propagation via the localization of gap junction proteins to the intercalated disks. Therefore, cardiomyocyte function must be directly related to its overall orientation and/or the orientation of its contractile proteins. Previous studies with hPSC-CMs have found that forced anisotropy results in cells with higher levels of sarcomere organization, contraction, maturation markers, and cytoskeletal anisotropy.[14,15,66,84]

In our studies, we chose to constrain hESC-CMs to varying degrees of anisotropy via extracellular matrix (ECM) patterning, to determine the range of pattern widths that promote the maturation of these cells. Anisotropy has previously been shown to result in cardiomyocytes with larger sarcomere lengths, smaller spread areas, and higher aspect

DOI: 10.1021/acsbiomaterials.8b01256
ACS Biomater. Sci. Eng. XXXX, XXX, XXX−XXX

Table 4. Comparison of Properties between Untreated hPSC-CMs, hPSC-CMs Exposed to Pro-maturation Stimuli, and Adult Human Cardiomyocytes[a]

property (unit)	hPSC-CM	stiffness	stiffness + anisotropy	stiffness + anisotropy + cell−cell contact	adult
cell area (μm^2)	480−800	1796	1600	1828	1820−2680
cell aspect ratio	1−2	1.9	3.7	4.1	7.5
binucleation (%)	4−18	15	12	33	26
sarcomere length (μm)	1.50−1.65	1.67	1.74	1.76	1.78−2.01
T_{Peak} (ms)	270−350	389	403	295	168−188
T_{Rel90} (ms)	791	653	646	469	209−337

[a]Here, the "stiffness" column indicates values for unpatterned hPSC-CMs on 21 kPa substrates, the "stiffness + anisotropy" column contains values for aligned cells on 21 kPa surfaces, and values in the "stiffness + anisotropy + cell−cell contact" column correspond to patterned cells seeded at high cell densities to induce cell−cell coupling. The hPSC-CM and adult cardiomyocyte data have been compiled from refs 4, 5, 70, 73, and 94−101.

ratios for both NRVMs[69,85] and hPSC-CMs.[14−16,66,86] Generally, these studies have found that the smaller the width of the anisotropy pattern, the larger the aspect ratio, longer the sarcomere length, and smaller the cell spread area. The effect of anisotropy on Z-band width is a less-explored topic. One study with NRVMs found that Z-widths were highest in aligned cells with aspect ratios in the range of 3−7,[68] while we found the highest Z-band widths on substrates with anisotropy patterns that yielded aspect ratios of 1:3 to 1:6. We are currently unaware of any other studies that have examined the effect of anisotropy on nuclear volume ratio or cell binucleation.

The forced anisotropy of RUES2 GCaMP3 hESC-CMs in our hands also led to changes in calcium handling properties (see Figure 7 and Table 2). Previous studies that have examined the effect of anisotropy on hiPSC-CM calcium handling properties have reported increases,[69,87] no effect,[15,88] or a reduction[16,89] in the maximal-to-basal calcium ratio. These same works reported inconsistent results regarding the effect of anisotropy on calcium transient times. One study found a reduction in T_{Peak} with anisotropy, but no changes in T_{50R} or T_{90R}.[88] Another found a reduction in T_{R90} but no change to T_{Peak}.[89] Other studies have reported no change in T_{Peak},[15] an increase in T_{50R},[16] and decreases to T_{peak} and relaxation time[87] in cardiomyocytes with altered anisotropy. Because of the inconsistent nature of these results, we cannot draw conclusive insights from those of our own study, except to say that that cell anisotropy alone does not appear to have a strong effect on calcium transient times of hPSC-CMs. To the best of our knowledge, no other studies have examined the effect of cellular anisotropy on the rates of calcium release and reuptake in hPSC-CMs.

4.3. Cell−Cell Contact. In the heart, cell−cell coupling is important for maintaining the normal function and development of the heart. Studies assessing the effect of cell−cell contact on cardiomyocytes in culture have found that membrane contact between cardiomyocytes is necessary for maintaining ion channel expression, coordinating cell polarization, and directing cell migration.[74,92] Furthermore, immature cardiomyocytes grown in an environment that promotes cell−cell contact have enhanced junctional protein expression, organization, and localization, as well as enhanced calcium dynamics, stronger contractile forces, and increased survival rates.[18,67,90,91,93] Based on these findings, we hypothesized that hESC-CMs grown in cell−cell contact on patterned surfaces would have enhanced structural and functional maturation.

Examination of the contractile structure revealed that hESC-CMs in cell−cell contact on the 18 μm pattern width had significantly longer sarcomeres than single hESC-CMs on the 24-μm pattern width. In addition, Z-band width was found to decrease with cell−cell contact on both pattern widths. The increased sarcomere length is likely an effect of the increased external stress on the cells. Regarding the shorter Z-band widths, it is possible that the stress from adjacent cells pulls the Z-bands out of register. However, given longer culture times, or with the addition of further pro-maturation stimuli, sarcomere lengths could increase and the Z-bands may realign.

Morphological analysis of hESC-CMs grown at high and low densities revealed that cell−cell contact within 24-μm width patterns led to significant increases in cell spread area, when compared to isolated cells or single cells grown in cell−cell contact on the 18-μm pattern width (see Figure 8). Since the average aspect ratio of these cells was not affected by cell−cell contact, we can conclude that these larger cells spread equally in the longitudinal and transverse directions. Cell−cell contact also yielded significant increases in the percentage of binucleated cells on both 18- and 24-μm pattern widths, as well as decreases in the nuclear volume ratio. Notably, while cell−cell contact stimulated binucleation on both pattern widths, cells on the 24-μm width reached binucleation levels equivalent to those seen in the adult myocardium. These results suggest that nuclear division in cardiomyocytes could be catalyzed by cell−cell contact. At this point, it is unclear whether this is due to the additional mechanical stress imposed on one cell by the other, because of chemical communication between the cells, or a combination of the two. Examination of the contractile structure revealed that hESC-CMs in cell−cell contact on the 18-μm pattern width had significantly longer sarcomeres than single hESC-CMs on the 24-μm pattern width, likely an effect of the increased external stress on the cells in cell−cell contact. It is possible that this stress acted to pull the cells' Z-bands out of register since Z-band width was found to decrease with cell−cell contact on both pattern widths.

Calcium transients of hESC-CMs in cell−cell contact (see Figure 9 and Table 3) showed slight increases in both normalized basal and maximal calcium intensity and showed significant decreases in the maximal-to-basal intensity ratio. Quantification of time to peak intensity, time to 50% calcium reuptake, and time to 90% calcium reuptake showed that cell−cell contact appears to result in faster calcium transient times. The rates of peak calcium release, 50% calcium reuptake, and 90% reuptake for cells on both pattern widths in cell−cell contact were seen to increase, albeit not significantly. These

DOI: 10.1021/acsbiomaterials.8b01256
ACS Biomater. Sci. Eng. XXXX, XXX, XXX−XXX

results suggest that not only are calcium transient times faster for hESC-CMs in cell−cell contact but the rates at which these signals travel throughout the entire cell area also increase. These calcium transients and rates were also found to be higher on the 24-μm pattern width, implying that increases in cell−cell contact area result in faster calcium handling.

4.4. Comparison to hPSC-CMs Grown under Standard Culture Conditions. This study demonstrated that optimizing the stiffness, anisotropy, and cell−cell contact of hESC-CMs led to positive modifications in the structural and functional state of these cells. In comparing the properties of these cells to those reported for hPSC-CMs grown in nonoptimized culture conditions, we find that each stimulus has a positive effect and that this combination was further improved by their downselected combination (see Table 4). We also found that this combination resulted in certain cellular properties reaching adult levels, while others have become much closer to adult in value. We hypothesize that adding additional stimuli on top of these will serve to further close the gap between the structural and functional properties of hPSC-CMs and adult human cardiomyocytes.

5. CONCLUSIONS

In this study, we examined the effect of combined pro-maturation stimuli on the structural and functional enhancement of hESC-CMs. To achieve this, a culture environment was created which allowed for alterations in environmental stiffness, anisotropy, and cell−cell contact. We found that hESC-CMs exposed to these stimuli, in parallel, were more structurally and functionally mature than those exposed to one or none. These findings support the notion that maturing hPSC-CMs to an adultlike state in vitro will require more than one strategy and advocate for combining the stimuli presented in this work with electrical, mechanical, and biochemical techniques, to achieve hPSC-CMs with the most advanced maturation state.

■ ASSOCIATED CONTENT

Supporting Information

The Supporting Information is available free of charge on the ACS Publications website at DOI: 10.1021/acsbiomaterials.8b01256.

Methods for obtaining and analyzing sarcomere orientation and laminin concentration measurements; effect of substrate stiffness on laminin concentration (Figure S1); effect of laminin line width on laminin concentration (Figure S2); effect of laminin line width on sarcomere organization (Figure S3) (PDF)

■ AUTHOR INFORMATION

Corresponding Author

*Tel.: (206) 685-6591. Fax: (206) 685-8047. E-mail: nsniadec@uw.edu.

ORCID

Nathan J. Sniadecki: 0000-0001-6960-4492

Author Contributions

M.L.R. and N.J.S. conceived and designed the experiments. M.L.R. performed the experiments. M.L.R., K.S.C., and K.M.B. analyzed the data. M.L.R., M.W., and X.Y.C. contributed reagents/materials/analysis tools; M.L.R. and K.M.B. created the figures. M.L.R., N.J.S., K.M.B., X.Y., and C.E.M. wrote the paper.

Funding

The authors wish to acknowledge support from the following sources: an NSF GRFP fellowship awarded to M.L.R., NIH Grant Nos. P01 HL094374, P01 GM081719, U01 HL100405, R01 HL084642 and U01 HL100395 (awarded to C.E.M.), and an NSF grant (No. CBET-1509106) that was awarded to N.J.S.

Notes

The authors declare the following competing financial interest(s): Charles Murry is a founder of and equity holder in Cytocardia, Inc. Nathan Sniadecki is a founder of and equity holder in Stasys Medical Corporation.

■ ACKNOWLEDGMENTS

Part of this work was conducted at the University of Washington's Washington Nanofabrication Facility, a member of the NSF National Nanotechnology Coordinated Infrastructure.

■ REFERENCES

(1) Matsa, E.; Denning, C. In vitro uses of human pluripotent stem cell-derived cardiomyocytes. *J. Cardiovasc. Transl. Res.* **2012**, *5*, 581−592.

(2) Yang, X.; Pabon, L.; Murry, C. E. Engineering adolescence: Maturation of human pluripotent stem cell-derived cardiomyocytes. *Circ. Res.* **2014**, *114*, 511−523.

(3) Robertson, C.; Tran, D. D.; George, S. C. Concise review: Maturation phases of human pluripotent stem cell-derived cardiomyocytes. *Stem Cells* **2013**, *31*, 829−837.

(4) Lundy, S. D.; Zhu, W.-Z.; Regnier, M.; Laflamme, M. A. Structural and Functional Maturation of Cardiomyocytes Derived from Human Pluripotent Stem Cells. *Stem Cells Dev.* **2013**, *22*, 1991−2002.

(5) Földes, G.; Mioulane, M.; Wright, J. S.; Liu, A. Q.; Novak, P.; Merkely, B.; Gorelik, J.; Schneider, M. D.; Ali, N. N.; Harding, S. E. Modulation of human embryonic stem cell-derived cardiomyocyte growth: A testbed for studying human cardiac hypertrophy? *J. Mol. Cell. Cardiol.* **2011**, *50*, 367−376.

(6) Shinozawa, T.; Imahashi, K.; Sawada, H.; Furukawa, H.; Takami, K. Determination of appropriate stage of human-induced pluripotent stem cell-derived cardiomyocytes for drug screening and pharmacological evaluation in vitro. *J. Biomol. Screening* **2012**, *17*, 1192−1203.

(7) Dias, T. P.; Pinto, S. N.; Santos, J. I.; Fernandes, T. G.; Fernandes, F.; Diogo, M. M.; Prieto, M.; Cabral, J. M. S. Biophysical study of human induced Pluripotent Stem Cell-Derived cardiomyocyte structural maturation during long-term culture. *Biochem. Biophys. Res. Commun.* **2018**, *499*, 611−617.

(8) Jung, G.; Fajardo, G.; Ribeiro, A. J. S.; Kooiker, K. B.; Coronado, M.; Zhao, M.; Hu, D.-Q.; Reddy, S.; Kodo, K.; Sriram, K.; Insel, P. A.; Wu, J. C.; Pruitt, B. L.; Bernstein, D. Time-dependent evolution of functional vs. remodeling signaling in induced pluripotent stem cell-derived cardiomyocytes and induced maturation with biomechanical stimulation. *FASEB J.* **2016**, *30*, 1464−1479.

(9) Feinberg, A. W.; Alford, P. W.; Jin, H.; Ripplinger, C. M.; Werdich, A. A.; Sheehy, S. P.; Grosberg, A.; Parker, K. K. Controlling the contractile strength of engineered cardiac muscle by hierarchal tissue architecture. *Biomaterials* **2012**, *33*, 5732−5741.

(10) McCain, M. L.; Parker, K. K. Mechanotransduction: The role of mechanical stress, myocyte shape, and cytoskeletal architecture on cardiac function. *Pfluegers Arch.* **2011**, *462*, 89−104.

(11) Geisse, N. A.; Sheehy, S. P.; Parker, K. K. Control of myocyte remodeling in vitro with engineered substrates. *In Vitro Cell. Dev. Biol.: Anim.* **2009**, *45*, 343−350.

DOI: 10.1021/acsbiomaterials.8b01256
ACS Biomater. Sci. Eng. XXXX, XXX, XXX−XXX

(12) Bray, M. A.; Sheehy, S. P.; Parker, K. K. Sarcomere alignment is regulated by myocyte shape. *Cell Motil. Cytoskeleton* **2008**, *65*, 641−651.
(13) Parker, K. K.; Tan, J.; Chen, C. S.; Tung, L. Myofibrillar architecture in engineered cardiac myocytes. *Circ. Res.* **2008**, *103*, 340−342.
(14) Wanjare, M.; Hou, L.; Nakayama, K. H.; Kim, J. J.; Mezak, N. P.; Abilez, O. J.; Tzatzalos, E.; Wu, J. C.; Huang, N. F. Anisotropic microfibrous scaffolds enhance the organization and function of cardiomyocytes derived from induced pluripotent stem cells. *Biomater. Sci.* **2017**, *5*, 1567−1578.
(15) Xu, C.; Wang, L.; Yu, Y.; Yin, F.; Zhang, X.; Jiang, L.; Qin, J. Bioinspired onion epithelium-like structure promotes the maturation of cardiomyocytes derived from human pluripotent stem cells. *Biomater. Sci.* **2017**, *5*, 1810−1819.
(16) Han, J.; Wu, Q.; Xia, Y.; Wagner, M. B.; Xu, C. Cell alignment induced by anisotropic electrospun fibrous scaffolds alone has limited effect on cardiomyocyte maturation. *Stem Cell Res.* **2016**, *16*, 740−750.
(17) Ribeiro, M. C.; Tertoolen, L. G.; Guadix, J. A.; Bellin, M.; Kosmidis, G.; D'Aniello, C.; Monshouwer-Kloots, J.; Goumans, M.-J.; Wang, Y.-L.; Feinberg, A. W.; Mummery, C. L.; Passier, R. Functional maturation of human pluripotent stem cell derived cardiomyocytes in vitro - Correlation between contraction force and electrophysiology. *Biomaterials* **2015**, *51*, 138−150.
(18) Pedrotty, D. M.; Klinger, R. Y.; Badie, N.; Hinds, S.; Kardashian, A.; Bursac, N. Structural coupling of cardiomyocytes and noncardiomyocytes: quantitative comparisons using a novel micropatterned cell pair assay. *AJP Hear. Circ. Physiol.* **2008**, *295*, H390−400.
(19) Werley, C. A.; Chien, M.-P.; Gaublomme, J.; Shekhar, K.; Butty, V.; Yi, B. A.; Kralj, J. M.; Bloxham, W.; Boyer, L. A.; Regev, A.; Cohen, A. E. Geometry-dependent functional changes in iPSC-derived cardiomyocytes probed by functional imaging and RNA sequencing. *PLoS One* **2017**, *12*, No. e0172671.
(20) Hersch, N.; Wolters, B.; Dreissen, G.; Springer, R.; Kirchgeßner, N.; Merkel, R.; Hoffmann, B. The constant beat: cardiomyocytes adapt their forces by equal contraction upon environmental stiffening. *Biol. Open* **2013**, *2*, 351−361.
(21) Jacot, J. G.; McCulloch, A. D.; Omens, J. H. Substrate stiffness affects the functional maturation of neonatal rat ventricular myocytes. *Biophys. J.* **2008**, *95*, 3479−3487.
(22) Jacot, J. C.; Martin, J. C.; Hunt, D. L. Mechanobiology of cardiomyocyte development. *J. Biomech.* **2010**, *43*, 93−98.
(23) van Deel, E. D.; Najafi, A.; Fontoura, D.; Valent, E.; Goebel, M.; Kardux, K.; Falcão-Pires, I.; van der Velden, J. In vitro model to study the effects of matrix stiffening on Ca2+handling and myofilament function in isolated adult rat cardiomyocytes. *J. Physiol.* **2017**, *595*, 4597−4610.
(24) Pasqualini, F. S.; Agarwal, A.; O'Connor, B. B.; Liu, Q.; Sheehy, S. P.; Parker, K. K. Traction force microscopy of engineered cardiac tissues. *PLoS One* **2018**, *13*, No. e0194706.
(25) Herron, T. J.; Da Rocha, A. M.; Campbell, K. F.; Ponce-Balbuena, D.; Willis, B. C.; Guerrero-Serna, G.; Liu, Q.; Klos, M.; Musa, H.; Zarzoso, M.; Bizy, A.; Furness, J.; Anumonwo, J.; Mironov, S.; Jalife, J. Extracellular matrix-mediated maturation of human pluripotent stem cell-derived cardiac monolayer structure and electrophysiological function. *Circ.: Arrhythmia Electrophysiol.* **2016**, *9*, No. e003638.
(26) Tallawi, M.; Rai, R.; Boccaccini, A. R.; Aifantis, K. E. Effect of Substrate Mechanics on Cardiomyocyte Maturation and Growth. *Tissue Eng., Part B* **2015**, *21*, 157−165.
(27) Dasbiswas, K.; Majkut, S.; Discher, D. E.; Safran, S. A. Substrate stiffness-modulated registry phase correlations in cardiomyocytes map structural order to coherent beating. *Nat. Commun.* **2015**, *6*, No. 6085.
(28) Fink, C.; Ergün, S.; Kralisch, D.; Remmers, U.; Weil, J.; Eschenhagen, T. Chronic stretch of engineered heart tissue induces hypertrophy and functional improvement. *FASEB J.* **2000**, *14*, 669−679.
(29) Throm Quinlan, A. M.; Sierad, L. N.; Capulli, A. K.; Firstenberg, L. E.; Billiar, K. L. Combining dynamic stretch and tunable stiffness to probe cell mechanobiology in vitro. *PLoS One* **2011**, *6*, No. e23272.
(30) Hülsmann, J.; Aubin, H.; Wehrmann, A.; Lichtenberg, A.; Akhyari, P. The Impact of Left Ventricular Stretching in Model Cultivations With Neonatal Cardiomyocytes in a Whole-Heart Bioreactor. *Biotechnol. Bioeng.* **2017**, *114*, 1107−1117.
(31) Xu, F.; Zhao, R.; Liu, A. S.; Metz, T.; Shi, Y.; Bose, P.; Reich, D. H. A microfabricated magnetic actuation device for mechanical conditioning of arrays of 3D microtissues. *Lab Chip* **2015**, *15*, 2496−2503.
(32) Kurazumi, H.; Kubo, M.; Ohshima, M.; Yamamoto, Y.; Takemoto, Y.; Suzuki, R.; Ikenaga, S.; Mikamo, A.; Udo, K.; Hamano, K.; Li, T. S. The effects of mechanical stress on the growth, differentiation, and paracrine factor production of cardiac stem cells. *PLoS One* **2011**, *6*, No. e28890.
(33) Gwak, S.; Bhang, S.; Kim, I.; Kim, S.; Cho, S.; Jeon, O.; Yoo, K.; Putnam, A.; Kim, B. The effect of cyclic strain on embryonic stem cell-derived cardiomyocytes. *Biomaterials* **2008**, *29*, 844−856.
(34) Shimko, V. F.; Claycomb, W. C. Effect of Mechanical Loading on Three-Dimensional Cultures of Embryonic Stem Cell-Derived Cardiomyocytes. *Tissue Eng., Part A* **2008**, *14*, 49−58.
(35) Cassino, T. R.; Drowley, L.; Okada, M.; Beckman, S. A.; Keller, B.; Tobita, K.; LeDuc, P. R.; Huard, J. Mechanical Loading of Stem Cells for Improvement of Transplantation Outcome in a Model of Acute Myocardial Infarction: The Role of Loading History. *Tissue Eng., Part A* **2012**, *18*, 1101−1108.
(36) Morgan, K. Y.; Black, L. D. Investigation into the effects of varying frequency of mechanical stimulation in a cycle-by-cycle manner on engineered cardiac construct function. *J. Tissue Eng. Regener. Med.* **2017**, *11*, 342−353.
(37) Mihic, A.; Li, J.; Miyagi, Y.; Gagliardi, M.; Li, S. H.; Zu, J.; Weisel, R. D.; Keller, G.; Li, R. K. The effect of cyclic stretch on maturation and 3D tissue formation of human embryonic stem cell-derived cardiomyocytes. *Biomaterials* **2014**, *35*, 2798−2808.
(38) Chun, Y. W.; Voyles, D. E.; Rath, R.; Hofmeister, L. H.; Boire, T. C.; Wilcox, H.; Lee, J. H.; Bellan, L. M.; Hong, C. C.; Sung, H.-J. Differential responses of induced pluripotent stem cell-derived cardiomyocytes to anisotropic strain depends on disease status. *J. Biomech.* **2015**, *48*, 3890−3896.
(39) Ruan, J.; Tulloch, N. L.; Saiget, M.; Paige, S. L.; Razumova, M. V.; Regnier, M.; Tung, K. C.; Keller, G.; Pabon, L.; Reinecke, H.; Murry, C. E. Mechanical Stress Promotes Maturation of Human Myocardium From Pluripotent Stem Cell-Derived Progenitors. *Stem Cells* **2015**, *33*, 2148−2157.
(40) Hirt, M. N.; Boeddinghaus, J.; Mitchell, A.; Schaaf, S.; Börnchen, C.; Müller, C.; Schulz, H.; Hubner, N.; Stenzig, J.; Stoehr, A.; Neuber, C.; Eder, A.; Luther, P. K.; Hansen, A.; Eschenhagen, T. Functional improvement and maturation of rat and human engineered heart tissue by chronic electrical stimulation. *J. Mol. Cell. Cardiol.* **2014**, *74*, 151−161.
(41) Eng, G.; Lee, B. W.; Protas, L.; Gagliardi, M.; Brown, K.; Kass, R. S.; Keller, G.; Robinson, R. B.; Vunjak-Novakovic, G. Autonomous beating rate adaptation in human stem cell-derived cardiomyocytes. *Nat. Commun.* **2016**, *7*, 10312.
(42) Sun, X.; Nunes, S. S. Biowire platform for maturation of human pluripotent stem cell-derived cardiomyocytes. *Methods* **2016**, *101*, 21−26.
(43) Zhang, N.; Stauffer, F.; Simona, B. R.; Zhang, F.; Zhang, Z. M.; Huang, N. P.; Vörös, J. Multifunctional 3D electrode platform for real-time in situ monitoring and stimulation of cardiac tissues. *Biosens. Bioelectron.* **2018**, *112*, 149−155.
(44) Baumgartner, S.; Halbach, M.; Krausgrill, B.; Maass, M.; Srinivasan, S. P.; Sahito, R. G. A.; Peinkofer, G.; Nguemo, F.; Müller-Ehmsen, J.; Hescheler, J. Electrophysiological and morphological maturation of murine fetal cardiomyocytes during electrical

DOI: 10.1021/acsbiomaterials.8b01256
ACS Biomater. Sci. Eng. XXXX, XXX, XXX−XXX

stimulation in vitro. *J. Cardiovasc. Pharmacol. Ther.* **2015**, *20*, 104−112.
(45) Korte, F. S.; Dai, J.; Buckley, K.; Feest, E. R.; Adamek, N.; Geeves, M. A.; Murry, C. E.; Regnier, M. Upregulation of cardiomyocyte ribonucleotide reductase increases intracellular 2 deoxy-ATP, contractility, and relaxation. *J. Mol. Cell. Cardiol.* **2011**, *51*, 894−901.
(46) Nowakowski, S. G.; Kolwicz, S. C.; Korte, F. S.; Luo, Z.; Robinson-Hamm, J. N.; Page, J. L.; Brozovich, F.; Weiss, R. S.; Tian, R.; Murry, C. E.; Regnier, M. Transgenic overexpression of ribonucleotide reductase improves cardiac performance. *Proc. Natl. Acad. Sci. U. S. A.* **2013**, *110*, 6187−6192.
(47) Lee, Y.-K.; Ng, K.-M.; Chan, Y.-C.; Lai, W.-H.; Au, K.-W.; Ho, C.-Y. J.; Wong, L.-Y.; Lau, C.-P.; Tse, H.-F.; Siu, C.-W. Triiodothyronine Promotes Cardiac Differentiation and Maturation of Embryonic Stem Cells via the Classical Genomic Pathway. *Mol. Endocrinol.* **2010**, *24*, 1728−1736.
(48) Shi, S. T.; Wu, X. X.; Hao, W.; Wang, X.; Miao, H. T.; Zhen, L.; Nie, S. P. Triiodo-l-Thyronine Promotes the Maturation of Cardiomyocytes Derived From Rat Bone Marrow Mesenchymal Stem Cells. *J. Cardiovasc. Pharmacol.* **2016**, *67*, 388−393.
(49) Kosmidis, G.; Bellin, M.; Ribeiro, M. C.; Van Meer, B.; Ward-Van Oostwaard, D.; Passier, R.; Tertoolen, L. G. J.; Mummery, C. L.; Casini, S. Altered calcium handling and increased contraction force in human embryonic stem cell derived cardiomyocytes following short term dexamethasone exposure. *Biochem. Biophys. Res. Commun.* **2015**, *467*, 998−1005.
(50) Parikh, S. S.; Blackwell, D. J.; Gomez-Hurtado, N.; Frisk, M.; Wang, L.; Kim, K.; Dahl, C. P.; Fiane, A.; Tønnessen, T.; Kryshtal, D. O.; Louch, W. E.; Knollmann, B. C. Thyroid and Glucocorticoid Hormones Promote Functional T-Tubule Development in Human-Induced Pluripotent Stem Cell-Derived Cardiomyocytes. *Circ. Res.* **2017**, *121*, 1323−1330.
(51) White, M. C.; Pang, L.; Yang, X. MicroRNA-mediated maturation of human pluripotent stem cell-derived cardiomyocytes: Towards a better model for cardiotoxicity? *Food Chem. Toxicol.* **2016**, *98*, 17−24.
(52) Kuppusamy, K. T.; Jones, D. C.; Sperber, H.; Madan, A.; Fischer, K. A.; Rodriguez, M. L.; Pabon, L.; Zhu, W.-Z.; Tulloch, N. L.; Yang, X.; Sniadecki, N. J.; Laflamme, M. A.; Ruzzo, W. L.; Murry, C. E.; Ruohola-Baker, H. Let-7 family of microRNA is required for maturation and adult-like metabolism in stem cell-derived cardiomyocytes. *Proc. Natl. Acad. Sci. U. S. A.* **2015**, *112*, E2785−2794.
(53) Yang, X.; Rodriguez, M. L.; Pabon, L.; Fischer, K. A.; Reinecke, H.; Regnier, M.; Sniadecki, N. J.; Ruohola-Baker, H.; Murry, C. E. Tri-iodo-L-thyronine promotes the maturation of human cardiomyocytes-derived from induced pluripotent stem cells. *J. Mol. Cell. Cardiol.* **2014**, *72*, 296−304.
(54) Miklas, J. W.; Nunes, S. S.; Sofla, A.; Reis, L. A.; Pahnke, A.; Xiao, Y.; Laschinger, C.; Radisic, M. Bioreactor for modulation of cardiac microtissue phenotype by combined static stretch and electrical stimulation. *Biofabrication* **2014**, *6*, 024113.
(55) Zimmermann, W. H.; Schneiderbanger, K.; Schubert, P.; Didie, M.; Münzel, F.; Heubach, J. F.; Kostin, S.; Neuhuber, W. L.; Eschenhagen, T. Tissue engineering of a differentiated cardiac muscle construct. *Circ. Res.* **2002**, *90*, 223−230.
(56) Gopalan, S. M.; Flaim, C.; Bhatia, S. N.; Hoshijima, M.; Knoell, R.; Chien, K. R.; Omens, J. H.; McCulloch, A. D. Anisotropic stretch-induced hypertrophy in neonatal ventricular myocytes micropatterned on deformable elastomers. *Biotechnol. Bioeng.* **2003**, *81*, 578−587.
(57) Wheelwright, M.; Win, Z.; Mikkila, J. L.; Amen, K. Y.; Alford, P. W.; Metzger, J. M. Investigation of human iPSC-derived cardiac myocyte functional maturation by single cell traction force microscopy. *PLoS One* **2018**, *13*, No. e0194909.
(58) Chong, J. J. H.; Yang, X.; Don, C. W.; Minami, E.; Liu, Y. W.; Weyers, J. J.; Mahoney, W. M.; Van Biber, B.; Cook, S. M.; Palpant, N. J.; Gantz, J. A.; Fugate, J. A.; Muskheli, V.; Gough, G. M.; Vogel, K. W.; Astley, C. A.; Hotchkiss, C. E.; Baldessari, A.; Pabon, L.; Reinecke, H.; Gill, E. A.; Nelson, V.; Kiem, H. P.; Laflamme, M. A.; Murry, C. E. Human embryonic-stem cell-derived cardiomyocytes regenerate non-human primate hearts. *Nature* **2014**, *510*, 273−277.
(59) Zhu, W.-Z.; Van Biber, B.; Laflamme, M. A. Methods for the Derivation and Use of Cardiomyocytes from Human Pluripotent Stem Cells. *Methods Mol. Biol.* **2011**, *767*, 419−431.
(60) Laflamme, M. A.; Chen, K. Y.; Naumova, A. V.; Muskheli, V.; Fugate, J. A.; Dupras, S. K.; Reinecke, H.; Xu, C.; Hassanipour, M.; Police, S.; O'Sullivan, C.; Collins, L.; Chen, Y.; Minami, E.; Gill, E. A.; Ueno, S.; Yuan, C.; Gold, J.; Murry, C. E. Cardiomyocytes derived from human embryonic stem cells in pro-survival factors enhance function of infarcted rat hearts. *Nat. Biotechnol.* **2007**, *25*, 1015−1024.
(61) Xu, C.; Police, S.; Hassanipour, M.; Li, Y.; Chen, Y.; Priest, C.; O'Sullivan, C.; Laflamme, M. A.; Zhu, W. Z.; Van Biber, B.; Hegerova, L.; Yang, J.; Delavan-Boorsma, K.; Davies, A.; Lebkowski, J.; Gold, J. D. Efficient generation and cryopreservation of cardiomyocytes derived from human embryonic stem cells. *Regener. Med.* **2011**, *6*, 53−66.
(62) Bhana, B.; Iyer, R. K.; Chen, W. L.; Zhao, R.; Sider, K. L.; Likhitpanichkul, M.; Simmons, C. A.; Radisic, M. Influence of substrate stiffness on the phenotype of heart cells. *Biotechnol. Bioeng.* **2010**, *105*, 1148−1160.
(63) Palchesko, R. N.; Zhang, L.; Sun, Y.; Feinberg, A. W. Development of Polydimethylsiloxane Substrates with Tunable Elastic Modulus to Study Cell Mechanobiology in Muscle and Nerve. *PLoS One* **2012**, *7*, No. e51499.
(64) Desai, R. A.; Rodriguez, N. M.; Chen, C. S. Stamp off to micropattern sparse, multicomponent features. *Methods Cell Biol.* **2014**, *119*, 3−16.
(65) Sniadecki, N. J.; Chen, C. S. Microfabricated Silicone Elastomeric Post Arrays for Measuring Traction Forces of Adherent Cells. *Methods Cell Biol.* **2007**, *83*, 313−328.
(66) Salick, M. R.; Napiwocki, B. N.; Sha, J.; Knight, G. T.; Chindhy, S. A.; Kamp, T. J.; Ashton, R. S.; Crone, W. C. Micropattern width dependent sarcomere development in human ESC-derived cardiomyocytes. *Biomaterials* **2014**, *35*, 4454−4464.
(67) Hampe, N.; Jonas, T.; Wolters, B.; Hersch, N.; Hoffmann, B.; Merkel, R. Defined 2-D microtissues on soft elastomeric silicone rubber using lift-off epoxy-membranes for biomechanical analyses. *Soft Matter* **2014**, *10*, 2431−2443.
(68) Kuo, P. L.; Lee, H.; Bray, M. A.; Geisse, N. A.; Huang, Y. T.; Adams, W. J.; Sheehy, S. P.; Parker, K. K. Myocyte shape regulates lateral registry of sarcomeres and contractility. *Am. J. Pathol.* **2012**, *181*, 2030−2037.
(69) Pong, T.; Adams, W. J.; Bray, M. A.; Feinberg, A. W.; Sheehy, S. P.; Werdich, A. A.; Parker, K. K. Hierarchical architecture influences calcium dynamics in engineered cardiac muscle. *Exp. Biol. Med.* **2011**, *236*, 366−373.
(70) Hazeltine, L. B.; Simmons, C. S.; Salick, M. R.; Lian, X.; Badur, M. G.; Han, W.; Delgado, S. M.; Wakatsuki, T.; Crone, W. C.; Pruitt, B. L.; Palecek, S. P. Effects of substrate mechanics on contractility of cardiomyocytes generated from human pluripotent stem cells. *Int. J. Cell Biol.* **2012**, *2012*, 508294.
(71) Ribeiro, A. J. S.; Ang, Y.-S.; Fu, J.-D.; Rivas, R. N.; Mohamed, T. M. A.; Higgs, G. C.; Srivastava, D.; Pruitt, B. L. Contractility of single cardiomyocytes differentiated from pluripotent stem cells depends on physiological shape and substrate stiffness. *Proc. Natl. Acad. Sci. U. S. A.* **2015**, *112*, 12705−12710.
(72) Radisic, M.; Park, H.; Shing, H.; Consi, T.; Schoen, F. J.; Langer, R.; Freed, L. E.; Vunjak-Novakovic, G. Functional assembly of engineered myocardium by electrical stimulation of cardiac myocytes cultured on scaffolds. *Proc. Natl. Acad. Sci. U. S. A.* **2004**, *101*, 18129−18134.
(73) Olivetti, G.; Cigola, E.; Maestri, R.; Corradi, D.; Lagrasta, C.; Gambert, S. R.; Anversa, P. Aging, cardiac hypertrophy and ischemic cardiomyopathy do not affect the proportion of mononucleated and multinucleated myocytes in the human heart. *J. Mol. Cell. Cardiol.* **1996**, *28*, 1463−1477.
(74) Chopra, A.; Tabdanov, E.; Patel, H.; Janmey, P. A.; Kresh, J. Y. Cardiac myocyte remodeling mediated by N-cadherin-dependent

DOI: 10.1021/acsbiomaterials.8b01256
ACS Biomater. Sci. Eng. XXXX, XXX, XXX−XXX

mechanosensing. *Am. J. Physiol Hear. Circ Physiol.* **2011**, *300*, H1252−H1266.
(75) Forte, G.; Pagliari, S.; Ebara, M.; Uto, K.; Van Tam, J. K.; Romanazzo, S.; Escobedo-Lucea, C.; Romano, E.; Di Nardo, P.; Traversa, E.; Aoyagi, T. Substrate Stiffness Modulates Gene Expression and Phenotype in Neonatal Cardiomyocytes In Vitro. *Tissue Eng., Part A* **2012**, *18*, 1837−1848.
(76) Heras-Bautista, C. O.; Katsen-Globa, A.; Schloerer, N. E.; Dieluweit, S.; Abd El Aziz, O. M.; Peinkofer, G.; Attia, W. A.; Khalil, M.; Brockmeier, K.; Hescheler, J.; Pfannkuche, K. The influence of physiological matrix conditions on permanent culture of induced pluripotent stem cell-derived cardiomyocytes. *Biomaterials* **2014**, *35*, 7374−7385.
(77) Herron, T. J.; Rocha, A. M.; Campbell, K. F.; Ponce-Balbuena, D.; Willis, B. C.; Guerrero-Serna, G.; Liu, Q.; Klos, M.; Musa, H.; Zarzoso, M.; Bizy, A.; Furness, J.; Anumonwo, J.; Mironov, S.; Jalife, J. Extracellular Matrix−Mediated Maturation of Human Pluripotent Stem Cell−Derived Cardiac Monolayer Structure and Electrophysiological Function. *Circ.: Arrhythmia Electrophysiol.* **2016**, *9*, No. e003638.
(78) Pandey, P.; Hawkes, W.; Hu, J.; Megone, W. V.; Gautrot, J.; Anilkumar, N.; Zhang, M.; Hirvonen, L.; Cox, S.; Ehler, E.; Hone, J.; Sheetz, M.; Iskratsch, T. Cardiomyocytes Sense Matrix Rigidity through a Combination of Muscle and Non-muscle Myosin Contractions. *Dev. Cell* **2018**, *44*, 326−336.
(79) Chopra, A.; Patel, A.; Shieh, A. C.; Janmey, P. A.; Kresh, J. Y. α-Catenin Localization and Sarcomere Self-Organization on N-Cadherin Adhesive Patterns Are Myocyte Contractility Driven. *PLoS One* **2012**, *7*, No. e47592.
(80) Georges, P. C.; Janmey, P. A. Cell type-specific response to growth on soft materials. *J. Appl. Physiol.* **2005**, *98*, 1547−1553.
(81) McCain, M. L.; Yuan, H.; Pasqualini, F. S.; Campbell, P. H.; Parker, K. K. Matrix elasticity regulates the optimal cardiac myocyte shape for contractility. *AJP Hear. Circ. Physiol.* **2014**, *306*, H1525−H1539.
(82) Jacot, J. G.; Kita-Matsuo, H.; Wei, K. A.; Chen, H. S. V.; Omens, J. H.; Mercola, M.; McCulloch, D. A. Cardiac myocyte force development during differentiation and maturation. *Ann. N. Y. Acad. Sci.* **2010**, *1188*, 121−127.
(83) Rodriguez, A. G.; Han, S. J.; Regnier, M.; Sniadecki, N. J. Substrate stiffness increases twitch power of neonatal cardiomyocytes in correlation with changes in myofibril structure and intracellular calcium. *Biophys. J.* **2011**, *101*, 2455−2464.
(84) Chen, A.; Lee, E.; Tu, R.; Santiago, K.; Grosberg, A.; Fowlkes, C.; Khine, M. Integrated platform for functional monitoring of biomimetic heart sheets derived from human pluripotent stem cells. *Biomaterials* **2014**, *35*, 675−683.
(85) Wu, Y.; Wang, L.; Guo, B.; Ma, P. X. Interwoven Aligned Conductive Nanofiber Yarn/Hydrogel Composite Scaffolds for Engineered 3D Cardiac Anisotropy. *ACS Nano* **2017**, *11*, 5646−5659.
(86) Wang, J.; Chen, A.; Lieu, D. K.; Karakikes, I.; Chen, G.; Keung, W.; Chan, C. W.; Hajjar, R. J.; Costa, K. D.; Khine, M.; Li, R. A. Effect of engineered anisotropy on the susceptibility of human pluripotent stem cell-derived ventricular cardiomyocytes to arrhythmias. *Biomaterials* **2013**, *34*, 8878−8886.
(87) Feinberg, A. W.; Ripplinger, C. M.; Van Der Meer, P.; Sheehy, S. P.; Domian, I.; Chien, K. R.; Parker, K. K. Functional differences in engineered myocardium from embryonic stem cell-derived versus neonatal cardiomyocytes. *Stem Cell Rep.* **2013**, *1*, 387−396.
(88) Rao, C.; Prodromakis, T.; Kolker, L.; Chaudhry, U. A. R.; Trantidou, T.; Sridhar, A.; Weekes, C.; Camelliti, P.; Harding, S. E.; Darzi, A.; Yacoub, M. H.; Athanasiou, T.; Terracciano, C. M. The effect of microgrooved culture substrates on calcium cycling of cardiac myocytes derived from human induced pluripotent stem cells. *Biomaterials* **2013**, *34*, 2399−2411.
(89) Khan, M.; Xu, Y.; Hua, S.; Johnson, J.; Belevych, A.; Janssen, P. M. L.; Gyorke, S.; Guan, J.; Angelos, M. G. Evaluation of changes in morphology and function of human induced pluripotent stem cell derived cardiomyocytes (hiPSC-CMs) cultured on an aligned-nanofiber cardiac patch. *PLoS One* **2015**, *10*, No. e0126338.
(90) Yasui, K.; Kada, K.; Hojo, M.; Lee, J.-K.; Kamiya, K.; Toyama, J.; Opthof, T.; Kodama, I. Cell-to-cell interaction prevents cell death in cultured neonatal rat ventricular myocytes. *Cardiovasc. Res.* **2000**, *48*, 68−76.
(91) Yamamoto, S.; Yasui, K.; Palade, P. T.; James, T. N. Spontaneous death of isolated adult rat cardiocytes in culture in association with internucleosomal cleavage of genomic DNA. *Apoptosis* **1997**, *2*, 178−188.
(92) Hershman, K. M.; Levitan, E. S. Cell-cell contact between adult rat cardiac myocytes regulates Kv1.5 and Kv4.2 K channel mRNA expression. *Am. J. Physiol.* **1998**, *275*, C1473−1480.
(93) Luo, Y.; Radice, G. L. Cadherin-mediated adhesion is essential for myofibril continuity across the plasma membrane but not for assembly of the contractile apparatus. *J. Cell Sci.* **2003**, *116*, 1471−1479.
(94) Prajapati, C.; Pölönen, R.-P.; Aalto-Setälä, K. Simultaneous recordings of action potentials and calcium transients from human induced pluripotent stem cell derived cardiomyocytes. *Biol. Open* **2018**, *7*, bio035030.
(95) Rodriguez, M. L.; Graham, B. T.; Pabon, L. M.; Han, S. J.; Murry, C. E.; Sniadecki, N. J. Measuring the Contractile Forces of Human Induced Pluripotent Stem Cell-Derived Cardiomyocytes With Arrays of Microposts. *J. Biomech. Eng.* **2014**, *136*, 051005.
(96) Liu, J.; Fu, J. D.; Siu, C. W.; Li, R. A. Functional Sarcoplasmic Reticulum for Calcium Handling of Human Embryonic Stem Cell-Derived Cardiomyocytes: Insights for Driven Maturation. *Stem Cells* **2007**, *25*, 3038−3044.
(97) Fu, J.; Wang, Y.-K.; Yang, M. T.; Desai, R. A.; Yu, X.; Liu, Z.; Chen, C. S. Mechanical regulation of cell function with geometrically modulated elastomeric substrates. *Nat. Methods* **2010**, *7*, 733−736.
(98) Piacentino, V.; Weber, C. R.; Chen, X.; Weisser-Thomas, J.; Margulies, K. B.; Bers, D. M.; Houser, S. R. Cellular basis of abnormal calcium transients of failing human ventricular myocytes. *Circ. Res.* **2003**, *92*, 651−658.
(99) Nguyen, N.; Nguyen, W.; Nguyenton, B.; Ratchada, P.; Page, G.; Miller, P. E.; Ghetti, A.; Abi-Gerges, N. Adult human primary cardiomyocyte-based model for the simultaneous prediction of drug-induced inotropic and pro-arrhythmia risk. *Front. Physiol.* **2017**, *8*, 1073.
(100) Gerdes, A. M.; Kellerman, S. E.; Moore, J. A.; Muffly, K. E.; Clark, L. C.; Reaves, P. Y.; Malec, K. B.; McKeown, P. P.; Schocken, D. D. Structural remodeling of cardiac myocytes in patients with ischemic cardiomyopathy. *Circulation* **1992**, *86*, 426−430.
(101) Paci, M.; Pölönen, R. P.; Cori, D.; Penttinen, K.; Aalto-Setälä, K.; Severi, S.; Hyttinen, J. Automatic optimization of an in silico model of human iPSC derived cardiomyocytes recapitulating calcium handling abnormalities. *Front. Physiol.* **2018**, *9*, 709.

DOI: 10.1021/acsbiomaterials.8b01256
ACS Biomater. Sci. Eng. XXXX, XXX, XXX−XXX